GYRUS AND SULCUS MODELLING UTILIZING A GENERIC TOPOGRAPHY ANALYSIS STRATEGY FOR PROCESSING ARBITRARILY ORIENTED 3D SURFACES

Gerald Zwettler[(a)], Werner Backfrieder[(a,b)]

[(a)]Bio- and Medical Informatics, Research and Development Department,
Upper Austria University of Applied Sciences, Austria
[(b)]School of Informatics/Communications/Media, Upper Austria University of Applied Sciences, Austria

[(a)]gerald.zwettler@fh-hagenberg.at, [(b)]werner.backfrieder@fh-hagenberg.at

ABSTRACT
Accurate and robust identification of the gyri and sulci of the human brain is a pre-requisite of high importance for modelling the brain surface and thus to facilitate quantitative measurements and novel classification concepts. In this work we introduce a watershed-inspired image processing strategy for topographical analysis of arbitrary surfaces in 3D. Thereby the object's topographical structure represented as depth profile is iteratively transformed into cyclic graph representations of both, the lowest and the highest characteristics of the particular shape. For graph analysis, the surface elements are partitioned according to their depth value. Neighbouring regions at different depth levels are iteratively merged. For region merging, the shape defining medial axes of the involved regions have to be connected by the optimum path with respect to a fitness function balancing shortness and minimal depth level changes of the solution.

Keywords: topographical surface analysis, cyclic graph representation, sulcus and gyrus classification

1. INTRODUCTION

The accurate quantification of metabolic processes from functional emission tomography imaging modalities like positron emission tomography (PET) and single photon emission computed tomography (SPECT) for diagnosis of neurodegenerative diseases necessitates a precise and patient-specific segmentation and classification of the brain. For segmentation and classification tasks, morphological image modalities as magnetic resonance imaging (MRI) have to be fused with the data acquired by functional emission imaging. Thus, the segmentations and classifications evaluated based on the anatomically-precise imaging modalities can be applied to the emission data, facilitating quantitative analysis of the metabolic activity with respect to pre-classified anatomical regions. The classification concept addressed in this work is the partitioning of gray and white brain matter according to the gyrus and sulcus characteristics.

Any computer-based functional or anatomical classification requires binary segmentation as pre-processing. Utilizing T1-weighted brain MRI data, segmentation of gray and white matter can be achieved, using *k-means* clustering (Kanungo et al. 2002; Ibanez et al. 2005) for determination of the tissue types to discriminate and region growing for ensuring connectedness.

Based on a binary segmentation of the brain surface, several strategies for sulcus and gyrus classification have been presented and published in the past. A morphologic closing operation, i.e. dilation followed by erosion, with subsequent subtraction of the original MRI data allows processing of the sulcus volume via 3D skeletonization for extraction of the sulcus and gyrus folds (Lohmann 1998). In contrast to applying Euclidean distances, the use of a geodesic depth profile accounts for complexity and partial occlusion of the sulcus folds (Kao et al. 2006).

Besides these morphologic concepts, curvature analysis of a surface mesh calculated from gray and white matter can be utilized for detection of the gyrus and sulcus course (Vivodtzev et al. 2003) with respect to convexity and concavity.

In this paper we present a generic strategy for topographic analysis of arbitrary shapes and transformation of the depth profiles into cyclic graph representations. Thereby we account for imbalances in the local depth profiles due to asymmetries and deformations of the brain. The minimum graph connecting all local maxima and minima respectively is calculated, normalizing the local depth levels similar to the watershed segmentation concept. Our strategy is perfectly applicable for the task of gyrus and sulcus modelling as concave and convex paths can be identified. Based on the graph representations of the sulcus and gyrus courses, modelling of the brain surface can be easily achieved via distance-based classification utilizing morphologic operators as presented and discussed in the following sections.

2. MEDICAL BASICS

Classification of the human brain can be accomplished at different levels of granularity. At a top level, the main anatomical structures, like *cerebrum*, *cerebellum* and the *brain stem* can be identified. The cerebrum is

subdivided into two hemispheres and the main anatomical components, like *white matter*, *gray matter*, *cerebro-spinal fluid* (CSF), *ventricle*, *fat*, *bones* and the arterial and venous *vessel systems* are demarcated. The brain tissue composed of white and gray matter is sub-classified into *frontal lobe*, *parietal lobe*, *occipital lobe* and some more, all specific areas responsible for diverse neurological functions of the body (Pschyrembel 2002). Each lobe comprehends several *gyrus* and *sulcus* areas, forming the brain surface. Thereby the gyri refer to the convex bulgs on the brain surface that are delimited by convex trenches, the so called sulci. The notable main sulci and gyri are named, listed and charted in anatomical atlases (Ono et al. 1990).

The topography of gyrus and sulcus characteristics is highly applicable for registration tasks in case of multi-modal image processing or follow-up examinations. Furthermore, modelling of the gyrus segments facilitates the quantitative analysis of metabolic activities with respect to defined anatomical structures.

3. DATA

For testing of the gyrus and sulcus modelling concept, *n=20* T1-weighted MRI datasets of simulated brainweb database (Cocosco et al. 1997; Kwan, Evans, and Pike 1999) and associated reference segmentations are used.

Further test runs and validations will be performed utilizing *n=12* anonymous multi-modal patient studies comprising morphologic image acquisitions (T1, T2, PD, …) as well as functional images (SPECT, PET).

4. METHODOLOGY

Prior to performing the analysis process, a binary representation of the targeting object's surface, not addressed in this work, and a 3D depth profile must be pre-processed.

4.1. Estimation of the Reference Shape

For calculation of the depth profile of an arbitrarily shaped object, the reference shape, i.e. the smoothed shape without the vales and ridges, must be estimated.

Processing a solid body with an approximately spherical shape, like the human brain, calculation of the 3D convex hull (Barber, Dobkin and Huhdanpaa 1996; Sonka, Hlavac and Boyle 2007) as reference shape is highly feasible, see Fig. 1.

For other more complex shapes, where a spherical approximation would be too imprecise, an alternative calculation of the reference shape is feasible. When calculating a winged-edge isosurface of a binary 3D body (Baumgart 1972; Baumgart 1975; Ritter 2007; MeVis 2011), utilizing the quality factor, allows steering of the smoothing effect by polygonal reduction, i.e. up to which level, vales and ridges should influence the depth profile calculation, see Fig. 2 (b). The resulting isosurface is projected back to regular 3D voxel grid for further processing. Furthermore, morphologic closing operations as dilation followed by erosion can be utilized for smoothing the surface and calculation of the reference shape, see Fig. 2 (c).

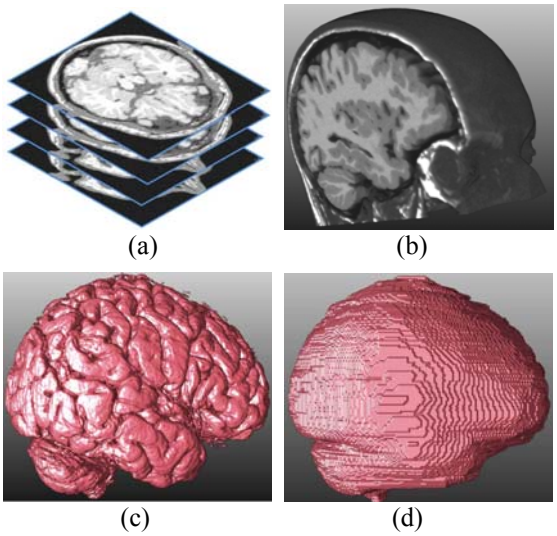

Figure 1: The stack of 2D MRI slices (a) assembles a 3D volume of the brain (b). After binary segmentation (c), the calculated convex hull (d) is the reference shape for depth profile calculation.

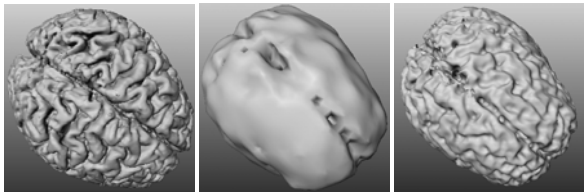

Figure 2: The precisely calculated surface model (a) can be smoothed for use as reference shape via rough isosurface calculation (b). As an alternative reference shape calculation strategy, a morphological closing operation with dilation kernel size *7x7x7* followed by erosion *6x6x6* can be applied (c).

4.2. Calculation of the Depth Profile

The depth profile is calculated as the minimum Euclidean distance between the surface of the object and the reference shape, see Fig. 3 as illustration of 2D depth profile calculation. A distance map calculation is used to represent the depth profile in 3D with the Euclidean neighbourhood weights for the adjacency constellations N_6, N_{12} and N_8 in *3x3x3* neighbourhood according to the distance from the hot spot as

$$w(N_6)=1.0\,;\; w(N_{12})=\sqrt{2}\,;\; w(N_8)=\sqrt{3}\,. \qquad (1)$$

Starting at the convex hull, the distance weights are propagated to the particular neighbours to set or update their values. Whenever the depth value of a neighbour gets adapted, the change is recursively propagated to all adjoined neighbours. Calculation of the depth profile is finished, when the depth value of each voxel refers to the minimal Euclidean distance from the convex hull.

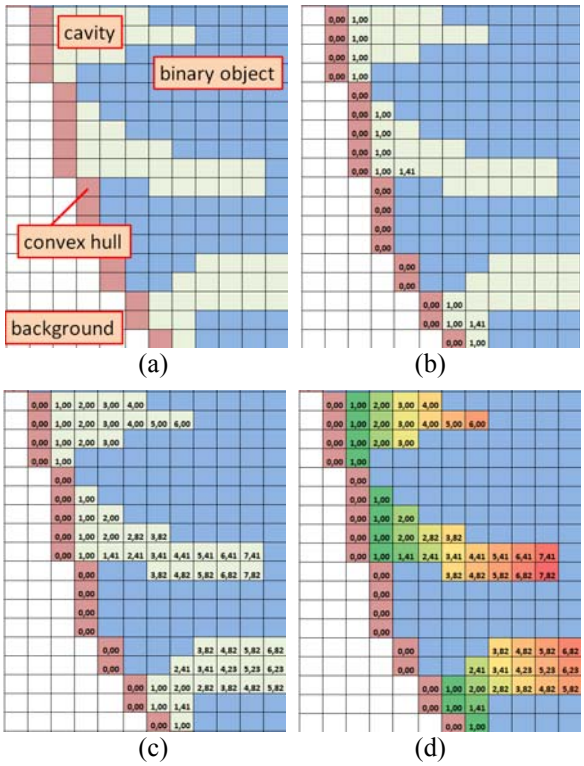

Figure 3: Calculation of the 2D depth profile for cavities between convex hull and the object's surface (a). In 2D case the neighbour weights are defined as $w(N_4)=1.0$ and $w(N_D)=1.41$. The depth profile is iteratively propagated until all depth values are calculated and convergence is reached (b-c). A colour-encoded representation of the final depth profile is plotted in (d).

The depth profile is calculated utilizing an Euclidean distance transform (Sonka, Hlavac and Boyle 2007). For calculation of the distance metrics, morphologic propagation of the outer surfaces, similar to the concept of grassfire transform (Blum 1967) is applied for fast approximate calculation of the Euclidean distance map from the object's borders. Results of the depth profile calculation are presented in Fig. 4. For the depth profile only the outer depth values below a threshold t are of relevance for gyrus and sulcus modelling. Depth profile values in the inner ventricular area are to exclude.

4.3. Watershed-Inspired Topography Analysis

Based on the calculated depth profile, the shortest graph interconnecting all local depth minimums is calculated, as well as a graph for connection of all local depth maxima. In the following delineation of the method, only the graph creation for the local maxima is addressed. The graph modelling for the local minimums can be derived by changing the leading signs and processing order.

The iterative process of graph construction is outlined in pseudo-code listing 1 and explained in detail in the following paragraphs.

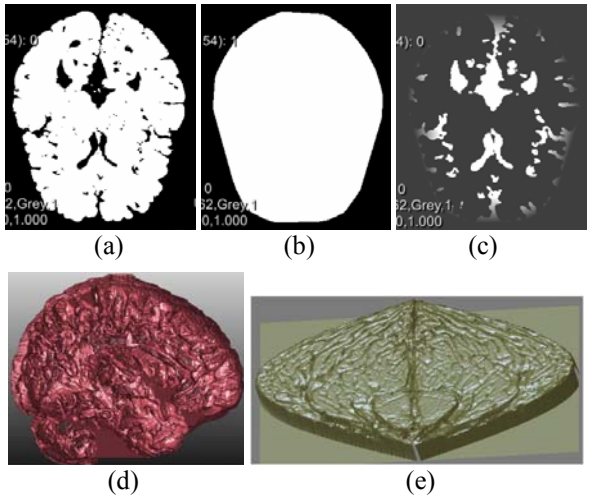

Figure 4: Planar representation of binary brain (a), convex hull (b) and depth profile (c) of mid slice transversal (axial) view. The 3D depth profile (d) as 2D map via Mollweide projection (Snyder 1987) is shown in (e).

The depth profile is processed at each particular depth level, starting at the maximum depth values and ending with the lowest depth values. At each depth level, voxels adjoined in N_{26} neighbourhood having matching depth values, are assembled together to recursively build up larger connected regions. For each of these constructed regions, the adjoined neighbourhood regions must be identified, differentiating between the following three constellations for the neighbourhood count N:

1. $N=0$: there are only background voxels or voxels at lower depth level not yet processed in the neighbourhood ➔ local maximum detected.
2. $N=1$: region is adjoined to one neighbouring region processed before with a higher depth value ➔ current region will be merged with the existing one.
3. $N>2$: there are several adjoined regions with higher depth values. The region to process is merged with the first neighbour region. Then the other neighbours are iteratively merged to one remaining cumulated region. Thereby, the skeleton sub-graphs must be interconnected.

For the autonomous regions to be interpreted as local maxima (condition 1), the first part of the graph is calculated via skeletonization. Below a region count of $R=50$ voxels, the region element closest to the centre of mass is taken as starting sub-branch of the graph, whereas for larger regions the medial axis, precisely extracted via skeletonization (Jonker 2002; Zwettler et al. 2009), is applied as starting sub-branch of the graph.

Regions with only one adjoined neighbouring region (condition 2), necessitate no discrete skeleton calculation. Instead, the region elements are just merged

with the neighbouring region, already defining a sub-branch.

If the current region is surrounded by more than one neighbour region at higher depth profile values (condition 3), besides a merge with the first neighbour region, all involved adjoined regions need to be cumulated. As all of the involved neighbouring regions have an already defined sub-part of the graph, these segments must be iteratively linked together. This link operation, described in the following sub-chapter, is a crucial task as it significantly influences the resulting graph after processing all depth levels from the deepest to the lowest profile values, see Fig. 5 for illustration of described iterative topography analysis. Starting at the deepest values with autonomous regions and the first skeleton parts Fig. 5 (c), the regions are enlarged whenever adjoined new regions at lower depth profile values are reached Fig. 5 (d-e). In case of reaching regions with already defined skeletons, the optimum connective path must be found Fig. 5 (f-g) utilizing detection of the optimal path, see Fig. 6. That way the topography describing path can be iteratively constructed until one final region remains Fig. 5 (h).

```
regions;
for(depth=maxVal; depth>=minVal; depth--)
  currRegions;
  for(xIdx=0; xIdx < sizeX; xIdx++)
    for(yIdx=0; yIdx < sizeY; yIdx++)
      for(zIdx=0; zIdx < sizeZ; zIdx++)
        if((distanceMap[xIdx][yIdx][zIdx] ==
            depth)&&
            (!classified(xIdx,yIdx,zIdx)))
          currRegions.Add(
            getRegionAt(xIdx,yIdx,zIdx));
  for(region : currRegions)
    neighbourRegions = getNeighbours(region);
    if(neighbourRegions.size == 0)
      region.CalculateSkeleton();
      regions.Add(region);
    else if(neighbourRegions.size == 1)
      merge(neighboruRegions.first, region)
    else
      merge(neighbourRegions.first, region)
      for (nRegion : neighbourRegions)
        if(nRegion != neighbourRegions.first)
          link_merge(
            neighbourRegions.first, nRegion)
```

Code Listing 1: Illustration of the topography analysis algorithm implemented in pseudo code. Regions at the same depth level are grouped together via region growing and stored in `currRegions`. Then for each region in `currRegions`, the neighbouring regions are identified. In case of neighbourhood *condition 1* with *N=0*, a seed region has been detected and the first skeleton is calculated. Seed regions are added to the global region container `regions`. If there is exactly one neighbouring region at higher depth level (*condition 2*), a region merging is performed. In case of additional neighbours (condition 3), the shortest skeleton path linking the involved regions is calculated prior to performing the merge operation.

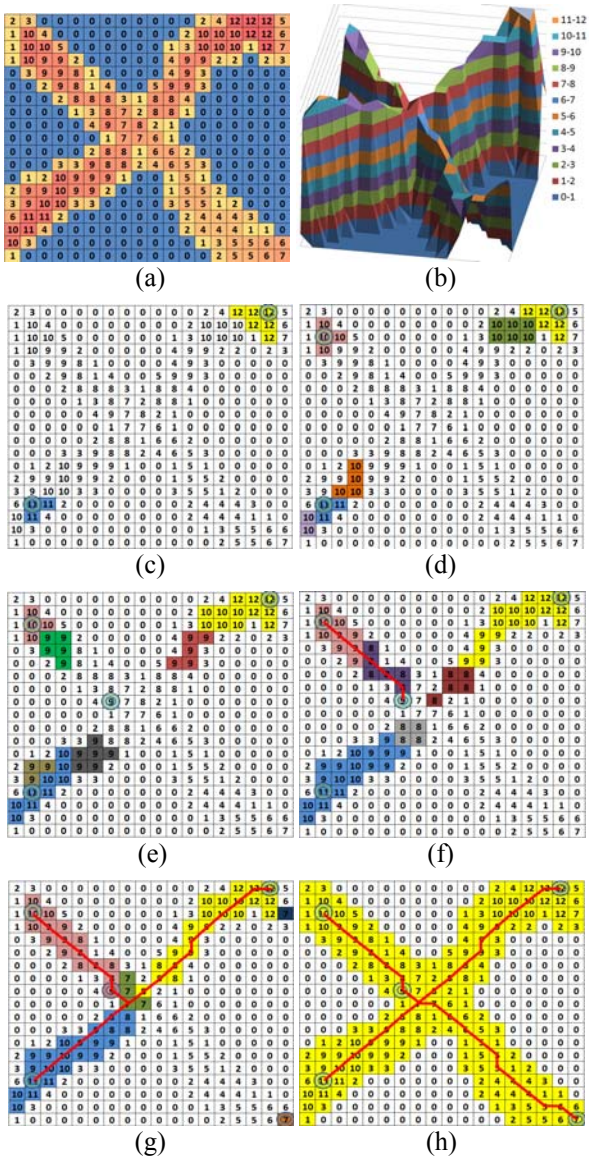

Figure 5: Illustration of the topography analysis on an cross-shaped 2D terrain.

4.3.1. Assembling Graph from Sub-Segments

When assembling two regions r_1 and r_2 with pre-calculated skeletons, i.e. graph sub-segments, the optimum path between the two skeletons $skel_1$ and $skel_2$ must be found. The search for the optimal connection path p_{min} is defined as minimization problem of a fitness function F, accounting for the Euclidean distance $dist()$ of the path and depth gradients of the path as $depth()$ with respect to the maximum profile depth $depth_{max}$, as

$$F(p) = \sum_{i=2}^{length(p)} \left(dist(p, i-1, i) \cdot \left(1 + depth_{\max} - depth(i)\right)\right). \quad (2)$$

Thereby the target path p_{min} is that path of all possible non-cyclic connections between $skel_1$ and $skel_2$ with a minimal value for F.

For calculation of the optimal path, the metric value F of the current sub-path is propagated to its neighbours, starting at the skeleton elements $skel_1$ of

region r_1. The sub-path fitness value is recursively propagated to the particular neighbours and updated for each added path element. Whenever the first element of $skel_2$ is reached, an upper border for the optimal path fitness value is given. That allows reduction in the calculation complexity as all sub-paths exceeding this upper border fitness value can be aborted.

After convergence of the fitness values is reached, the optimum path can be traced back starting at the element e_2 of skeleton $skel_2$ with an adjoined neighbour showing the lowest fitness. Starting at e_2 the way to skeleton $skel_1$ is traced back by selecting the element with lowest fitness in each particular neighbourhood. The optimal path is finished, when the first neighbour of $skel_1$ has been reached. The described algorithm is illustrated in Fig. 6.

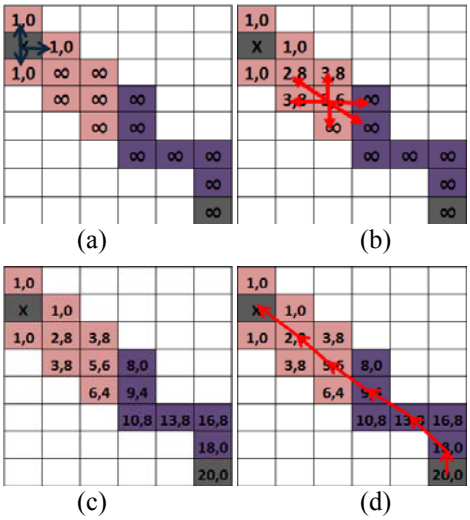

Figure 6: Detection of the optimal path between the two regions in Fig. 5 (f). Starting at the skeleton of the first region, all neighbours in N_8 are set or updated with the minimal path value according to the metrics defined in Eq. 2. Whenever a path value gets changed, all adjoined neighbours must be checked for propagation of the new value (b). Finally the path connecting the skeletons $skel_1$ and $skel_2$ can be traced back by picking each neighbour with the lowest value until skeleton of r_1 is reached (d).

5. RESULTS

In this chapter first results of the discussed method are presented and discussed.

5.1. Results of Sulcus Classification

The graph model resulting from sulcus classification highly correlates with the main anatomical folds, see Fig. 7. Some pruning and smoothing operations on the graph can be utilized in future to remove dispensable bifurcations and redundant node elements.

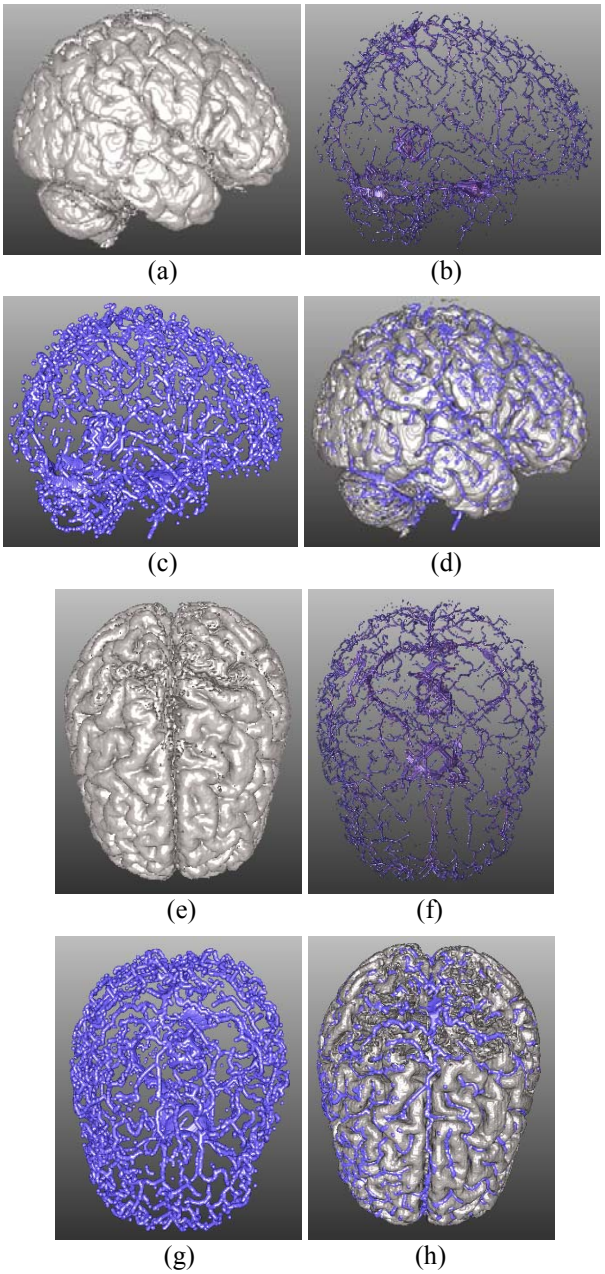

Figure 7: Visualization of sulcus analysis results in sagittal view (a-d) and axial view (e-h). The resulting tree model for the sulcus folds (b)(f) is amplified via morphologic dilation operation utilizing a 3x3x3 structuring element for better visibility (c)(g). Correlation of original brain surface (a)(e) and the sulcus models is presented in (d)(h) via overlay.

As our presented algorithm only interconnects adjoined region skeletons bridging shallow sections, foreshortening could arise if the depth profile is strictly monotonic increasing. That problem can only be exploited by processing artificial testing data. As the first results show, even minimal deflection from strict monotonic behaviour prevents any foreshortening of the particular sub-branch, processing real-world medical image data.

6. DISCUSSION AND CONCLUSIONS

In this paper we introduce a novel concept for classification of the gyrus and sulcus folds and representation as graph model.

The presented iterative topography analysis with step-wise assembling and interconnecting the final graph allows handling of local imbalances of the depth profile, e.g. due to deformation or asymmetries of the brain. Besides roughly estimated upper threshold value for the profile depth to process with respect to imaging resolution, no further parameterization is required.

Linking the final graph representations and the depth profile allows later restrictions on the granularity of sulcus and gyrus representation.

Utilizing the presented sulcus and gyrus graph models, classification of the brain areas can be easily achieved by iterative assigning the gray matter and white matter voxels to the closest neighbouring sub-trees, similar to vascularization-based anatomy classification (Zwettler, Backfrieder and Pichler 2011). Thereby the gyrus course can be used for iterative classification of the surrounding tissue and the sulcus lines are incorporated as additional barriers to prevent invalid merging of adjoined brain sections.

ACKNOWLEDGMENTS

Thanks to our medical partners from the Wagner-Jauregg state mental hospital, Linz, Upper Austria, at the institute for neuro-nuclear medicine headed by MD Robert Pichler for providing medical image data and valuable discussion.

This research is part of the INVERSIA project (http://inversia.fh-linz.at) which was funded by the European Regional Development Fund (ERDF) in cooperation with the Upper Austrian state government (REGIO 13).

REFERENCES

Barber, C.B., Dobkin, D.P., Huhdanpaa, H., 1996. The Quickhull Algorithm for Convex Hulls. In *ACM Transactions on Mathematical Software (TOMS)*.

Baumgart, B.G., 1972. Winged-Edge Polyhedron Representation, *Stanford University Artificial Intelligence Report No. CS-320*.

Baumgart, B.G., 1975. Polyhedral Representation for Computer Vision. In *Proc. of the National Computer Conference*, 589-596.

Blum, H., 1967. A Transformation for Extracting New Descriptors of Shape. In Wathen-Dunn, W., eds. *Models for the Perception of Speech and Visual Form*. MIT Press, Cambridge, 362-380.

Cocosco, C.A., Kollokian, V., Kwan, R.K.-S., Evans, A.C., 1997. BrainWeb: Online Interface to a 3D MRI Simulated Brain Database. Proceedings of the *3-rd International Conference on Functional Mapping of the Human Brain*, 5(4):425.

Ibanez, L., Schroeder, W., Ng., L., Cates, J., 2005. *The ITK Software Guide*. Kitware Inc.

Jonker, P.P., 2002. Skeletons in N dimensions using shape primitives. *Pattern Recognition Letters*, 23:677-686.

Kanungo, T., Mount, D.M., Netanyahu, N., Piatko, C., Silverman, R., Wu, Y.A., 2002. An efficient k-means clustering algorithm – Analysis and implementation. In: *IEEE Transactions on Pattern Analysis and Machine Intelligence*, 24:881-892.

Kao, C.-Y., Hofer, M., Sapiro, G., Stern, J., Rottenberg, D., 2006. A Geometric Method for Automatic Extraction of Sulcal Fundi. In: *IEEE International Symposium Biomedical Imaging*, 1168-1171.

Kwan, R.K.-S., Evans, A.C., Pike, G.B., 1999. MRI simulation-based evaluation of image-processing and classification methods. *IEEE Transactions on Medical Imaging*, 18(11):1085-1097.

Lohmann, G., 1998. Extracting Line Representations of Sulcal and Gyral Patterns in MR Images of the Human Brain. In: *IEEE Transactions on Medical Imaging* 17(6):1040-1048.

MeVis, 2011. *MeVisLab – medical image processing and visualization*, MeVis Medical Solutions, Bremen, Germany. Available from http://www.mevislab.de/developer/documentation/ [04/2011].

Ono, M., Kubick, S., Abernathey, C.D., 1990. *Atlas of the cerebral sulci*. Thieme publisher

Pschyrembel, W., 2002. *Pschyrembel klinisches Wörterbuch*. De Gruyter, Berlin, Germany.

Ritter, F., 2007. Visual Programming for Prototyping of Medical Applications. In *IEEE Visualization 2007* workshop.

Snyder, J.P., 1987. Map Projections – A Working Manual. In: *U.S: Geological Survey Professional Paper 1395*, Washington DC., U.S. Government Printing Office.

Sonka, M., Hlavac, V., Boyle, R., 2007. *Image Processing, Analysis, and Machine Vision*. Cengage Learning, 3rd edition.

Vivodtzev, F., Linsen, L., Bonneau, G.-P., Hamann, B., Joy, K.I., Olshausen, B.A.,2003. Hierarchical Isosurface Segmentation Based on Discrete Curvature. In: *Joint EUROGRAPHICS – IEE TCVG Symposium on Visualization*, 249-258.

Zwettler, G.A., Swoboda, R., Pfeifer, F., Backfrieder, W., 2009. Fast Medial Axis Extraction Algorithm on Tubular Large 3D Data by Randomized Erosion. In: Ranchordas, A.K., Araujo, H.J., Pereira, J.M., Braz, J., eds. *Computer Vision and Computer Graphics – Communications in Computer and Information Science*. Springer Publisher, 24:97-108.

Zwettler, G., Backfrieder, W., Pichler, R., 2011. Diagnosis of Neurodegenerative Diseases based on Multi-modal Hemodynamic Classification of the Brain. In *Proceedings of the International Conference on Computer Aided Systems Theory EUROCAST 2011*, 363-365.

AUTHORS BIOGRAPHY

Gerald A. Zwettler was born in Wels, Austria and attended the Upper Austrian University of Applied Sciences, Campus Hagenberg where he studied software engineering for medicine and graduated Dipl.-Ing.(FH) in 2005 and the follow up master studies in software engineering in 2009. In 2010 he has started his PhD studies at the University of Vienna at the Institute of Scientific Computing. Since 2005 he is working as research and teaching assistant at the Upper Austrian University of Applied Sciences at the school of informatics, communications and media at the Campus Hagenberg in the field of medical image analysis and software engineering with focus on computer-based diagnostics support and medical applications. His e-mail address is gerald.zwettler@fh-hagenberg.at and the research web page of the Research & Development department at campus Hagenberg, he is employed at, can be found under the link http://www.fh-ooe.at/fe/forschung.

Werner Backfrieder received his degree in technical physics at the Vienna University of Technology in 1992. Then he was with the Department of Biomedical Engineering and Physics of the Medical University of Vienna, where he reached a tenure position in 2002. Since 2002 he is with the University of Applied Sciences Upper Austria at the division of Biomedical Informatics. His research focus is on Medical Physics and Medical Image Processing in Nuclear Medicine and Radiology with emphasis to high performance computing. Recently research efforts were laid on virtual reality techniques in the context of surgical planning and navigation.